Nanoscale

An integrated experimental and theoretical study on optical properties of uniform hairy noble metal nanoparticles

Journal:	*Nanoscale*
Manuscript ID	NR-ART-09-2018-007115.R1
Article Type:	Paper
Date Submitted by the Author:	30-Sep-2018
Complete List of Authors:	Yang, Di; Minzu University of China, Chen, Yihuang; Georgia Institute of Technology, School of Materials Science and Engineering Peng , Hong-Shang ; School of Science, Minzu University of China Chen, Genxiang; Minzu University of China, School of Science Lin, Zhiqun; Georgia Institute of Technology, Materials Science and Engineering

SCHOLARONE™
Manuscripts

Cite this: DOI: 10.1039/c1ee00000x

www.rsc.org/ees

PAPER

An integrated experimental and theoretical study on optical properties of uniform hairy noble metal nanoparticles

Di Yang,†,[1] Yihuang Chen,†,[2] Hongshang Peng,[1] Gengxiang Chen,[1] and Zhiqun Lin*,[2]

†Equal contribution

[1]School of Science, Minzu University of China, Beijing 100081, China

[2]School of Materials Science and Engineering, Georgia Institute of Technology, Atlanta, GA 30332

Received (in XXX, XXX) Xth XXXXXXXXX 20XX, Accepted Xth XXXXXXXXX 20XX
DOI: 10.1039/c1ee00000x

We report a viable route to plasmonic nanoparticles with well-controlled sizes, shapes, and compositions. A series of monodisperse Ag and Au nanoparticles capped with polystyrene chains (i.e., "hairy" nanoparticles) are crafted by capitalizing on star-like diblock copolymers as nanoreactors. Such monodisperse nanoparticles render an accurate absorption spectrum, providing a strong basis for theoretical investigation into their optical properties. By combining experimental study with three-dimensional finite element calculation of electromagnetic field distributions, the contributions of both intra-band and inter-band transitions to plasmonic absorption are revealed. The calculated absorption spectra perfectly reproduce the experimental observations, including peak positions, shapes, and trends of peak shifting or broadening as a function of nanoparticle sizes. The influences of nanoparticle dimensions and surface ligands on plasmonic absorption of metallic nanoparticles are also systematically explored.

1. Introduction

Colloidal noble metal nanoparticles (i.e., Ag and Au) exhibit intriguing optical frequencies due to strong surface plasmon resonance (SPR) at optical frequencies[1-3] for a wide range of applications in surface-enhanced sensing and spectroscopy,[4,5] high-resolution imaging,[6] light localization and guiding,[7] photocatalysis,[3,8] transport and storage of energy,[9-11] and optical force enhancement in nanoaggregates.[12] Interestingly, physical and chemical properties of plasmonic nanoparticles consisting of a few hundred up to several thousand atoms can be perfectly regulated by the geometric and compositional engineering during synthesis to meet the requirements of relevant applications, for example, as building blocks for functional materials and devices.[13-17] Recently, controllable preparative strategy to precisely tailor the dimension and composition of plasmonic nanoparticles with high stability has been a topic of general interest. The traditional solution-based colloidal synthesis has been widely used to produce plasmonic nanoparticles.[18] Surface passivation of nanoparticle with ligands (e.g., small molecular surfactants and linear polymers) during their synthesis is an indispensable procedure in preventing them from agglomeration. However, the ligands tend to dissociate from the nanoparticle surface if experimental conditions (e.g., pH, temperature, UV irradiation, etc.) are changed. Thus, incomplete and uncontrollable surface coverage or ununiformity of polymers on the nanoparticle surface occurs, leading to the inhomogeneity of nanoparticles. Recently, nanoparticles have been prepared by using conventional micelles from self-assembly of linear amphiphilic block copolymer.[19] However, it is difficult to maintain the shape as characteristics of the micelles for a given system depend heavily on temperature, solvent properties, etc.[20,21] To this end, we have recently developed a facile strategy for creating high-quality plasmonic nanoparticles by judiciously exploiting amphiphilic star-like copolymers with well-defined molecular architecture and molecular weight as nanoreactors.[15,22,23] In stark contrast to the conventional method for synthesizing nanoparticles capped with small ligands via relatively weak interaction, nanoparticles produced via amphiphilic star-like copolymer strategy are intimately and permanently capped with a layer of polymer chains, resulting in excellent solubility in nonpolar solvents with prolonged stability. Moreover, the dimensions and compositions of monodisperse nanoparticles can be easily adjusted by tailoring the molecular weights of the polymer template and choosing proper precursors for inorganic synthesis, respectively.

Over the past decades, theoretical investigation into the SPR of plasmonic nanoparticles has been actively invoked to provide a better guidance to experimental study.[24-30] However, some factors affecting the SPR of plasmonic nanoparticles have not yet fully understood and often been neglected in simulation. This is mainly reflected by a large discrepancy between calculated and experimental plasmonic absorptions. It is well-known that the existence of SPR is due to the coupling of electromagnetic waves to the motion of electrons. However, when characterizing the SPR of plasmonic nanoparticles, only transition motions of free electrons within an energy band, called intra-band excitations, are usually considered, while the influence of inter-band excitations is ignored (see *Supplementary Information* for intra-band excitation and inter-band excitation).[31-33] Recently, the effect of inter-band oscillations in the nonlinear optics of plasmonic nanocomposites has received much attention.[34,35] For instance, the metal-sapphire nanostructure was reported to enhance the incident laser field by means of SPR in which the inter- and intra-

band oscillations of electrons are supposed to be involved, triggering plasmonic high-harmonic generation directly.[35] Notably, the contributions from inter- and intra-band transitions to the plasmonic absorption of plasmonic nanoparticles have been theoretically investigated in several reports,[36] yet lack of experimental support.

Herein, we report the crafting of a series of monodisperse Ag and Au nanoparticles by exploiting amphiphilic nonlinear block copolymers as nanoreactors, and subsequent scrutiny of the effects of the intra- and inter-band transitions on the SPR of these monodisperse plasmonic nanoparticles. The correlation between the nanoparticle sizes and the corresponding plasmonic absorptions is demonstrated experimentally. Moreover, the environment-dependence of plasmonic absorption is studied via rationally varying the surface ligands situated on the surface of plasmonic nanoparticles. As the experimental results are derived from monodisperse plasmonic nanoparticles, they provide a good feedback for theoretical investigation into the SPR of plasmonic nanoparticles. Thus, by combining the systematically measured absorption spectra of plasmonic nanoparticles with the simulated absorption spectra calculated by 3-dimensional finite element method, the influences of the intra- and inter-band transitions on their SPR are explored. More importantly, an integrated experiment and modelling study reveals the influences of dimensions and surface ligands of Ag and Au nanoparticles on the plasmonic absorption.

2. Experimental Section

2.1 Synthesis of PS-capped Au and Ag nanoparticles

A series of monodisperse Ag and Au nanoparticles capped with polystyrene chains (i.e., *hairy* nanoparticles) were crafted by capitalizing on amphiphilic star-like poly(acrylic acid)-block-polystyrene (PAA-*b*-PS) diblock copolymers as nanoreactors based on our previous work.[23] The key to precisely control diameter and shape of Ag and Au nanoparticles is the rational design and synthesis of PAA-*b*-PS diblock copolymers with well-defined molecular weights and narrow molecular weight distributions.[22,23] First, heptakis[2,3,6-tri-O-(2-bromo-2-methylpropionyl)]-β-cyclodextrin (denoted 21Br-β-CD) was prepared.[23,37] Star-like PAA-b-PS diblock copolymer was then synthesized by atom transfer radical polymerization (ATRP) of tert-butyl acrylate and styrene in sequence using 21Br-β-CD as the macroinitiator, followed by the hydrolysis using trifluoroacetic acid.[23] Using star-like PAA-b-PS diblock copolymers as nanoreactors in a 10-ml mixed solvent containing dimethylformamide (DMF) and benzyl alcohol (BA) at the 9:1 ratio by volume, PS-capped noble metal nanoparticles were obtained with proper precursors (i.e., $AgNO_3$ for Ag nanoparticles and $HAuCl_4 \cdot 3H_2O$ for Au nanoparticles). These metallic nanoparticles were found to be highly crystalline.[23]

2.2 Theoretical calculations

The complex dielectric function is an important parameter to express the interaction between materials and light waves. In a complex dielectric function, the portion of inter-band transition and intra-band transition can be described by the Lorentz model[38] and the Drude model[39], respectively. Therefore, the complex dielectric function of nobel metals $\varepsilon(\omega) = \varepsilon_1(\omega) + \varepsilon_2(\omega)$. can be separated into two contributions associated with inter-band and intra-band transitions, respectively, $\varepsilon(\omega) = \varepsilon_{interband}(\omega) + \varepsilon_{intraband}(\omega)$.[38] The contribution of inter-band transition to the dielectric function is described by the simple semi-quantum model, resembling the Lorentz model:[38]

$$\varepsilon_{interband}(\omega) = \sum_{j=1}^{N} \frac{f_j \Omega_p^2}{\omega_j^2 - \omega^2 - i\omega\gamma_j} \quad (1)$$

where Ω_p denotes the plasma frequency associated with inter-band transition, and N is the number of resonances with the frequency ω_j, strength f_j, and damping constant γ_j. These parameters for Ag and Au used here are obtained from the report in which metallic optical parameters were obtained on the basis of the measured spectra of metallic films.[38] The contribution of intra-band transition to the dielectric function can be derived by the Drude model.[39] Since the particle size of metallic nanoparticles is comparable to the mean free path of free-electrons, the finite size effect needs to be taken into account. The modification of the finite size effect in the dielectric function is achieved by increasing a size-dependent factor $\frac{AV_f}{L_{eff}}$ to the bulk damping rate of free-electron γ_{D0}. Consequently, the modified damping rate of free-electron is given by $\gamma = \gamma_{D0} + \frac{AV_f}{L_{eff}}$, where V_f is the Fermi velocity of electron, L_{eff} the effective mean free path of electron, and A the proportionality factor. L_{eff} depends on the size and shape of nanoparticles and can be calculated for different shaped nanoparticles using $L_{eff} = 4V/S$, where V and S are the volume and surface area of nanoparticles, respectively. The modified Drude model is given as follows[40]

$$\varepsilon_{intraband} = 1 - \frac{\omega_p^2}{\omega^2 + i\omega\left(\gamma_{D0} + \frac{AV_f}{L_{eff}}\right)} = 1 - \frac{\omega_p^2}{\omega^2 + \left(\gamma_{D0} + \frac{AV_f}{L_{eff}}\right)^2} + i\frac{\omega_p^2}{\omega^3}\left[\frac{\left(\gamma_{D0} + \frac{AV_f}{L_{eff}}\right)}{1 + \frac{\left(\gamma_{D0} + \frac{AV_f}{L_{eff}}\right)^2}{\omega^2}}\right] \quad (2)$$

where ω_p is the plasma frequency associated with the intra-band transition. For Ag, ω_p, γ_{D0}, and V_f are 9.04 eV, 0.02125 eV and 1.39×10^6 m/s, respectively[41]. For Au, ω_p, γ_{D0} and V_f are 8.89 eV, 0.07088 eV and 1.40×10^6 m/s, respectively.[41] The proportionality factor A corresponds to an introduction of correction to errors in $\varepsilon_{intraband}$ and can directly be deduced by fitting the measured spectra.[42] In the study, A was set to 0.1 according to the measured spectra. In order to facilitate comparison, the A-value remained 0.1 for Ag and Au nanoparticles with various dimensions.

The relationship of $\omega \gg \left(\gamma_{D0} + \frac{AV_f}{L_{eff}}\right)$ exists at optical frequencies, the finite size effect noted above mainly influences the imaginary part of $\varepsilon_{intraband}$ according to the equation (2), which has also been verified in the literature.[43] Moreover, on the basis of the Kramers-Kronig relation, the real part of complex dielectric contants $\varepsilon_1(\omega)$ changes slightly if the size of Ag particles decrease, whereas the imaginary part $\varepsilon_2(\omega)$ is markedly enhanced (up to the tenfold of the bulk value).[44] Therefore, in our calculations on plasmonic nanoparticles, $\varepsilon_1(\omega)$ was fixed to the real component of $\varepsilon_{interband}(\omega) + \varepsilon_{intraband}(\omega)$, while $\varepsilon_2(\omega)$ was changed (i.e., set as the imaginary component of $\varepsilon_{intraband}(\omega)$ or the sum of $\varepsilon_{interband}(\omega) + \varepsilon_{intraband}(\omega)$) to explore the mechanism of the plasmonic absorption of metallic nanoparticles.

The extinction cross-sections (δ_{ext}) is defined as the sum of the absorption cross-section (δ_{abs}) and the scattering cross-section (δ_{sca}). For the small-sized colloidal nanoparticles investigated in this work, the absorption dominates over the scattering by approximately 100 times, so $\delta_{sca} = \delta_{abs} + \delta_{sca} \approx \delta_{abs}$.[45] The absorption cross-section (δ_{abs}) of nanoparticles can be obtained by integrating the absorbed power density over the entire volume (V) of the metallic part:[45]

$$\delta_{abs}(\omega) = \frac{2}{c\varepsilon_0}\int_V [\sigma(\omega)E \cdot E^* - i\omega E \cdot D^*]\mathrm{d}V \quad (3)$$

This journal is © The Royal Society of Chemistry 2013

where, $\boldsymbol{E}$, $\boldsymbol{D}$, and σ are the electric field intensity, electric displacement, and electric conductivity, respectively. The 3-dimensional calculation of electromagnetic field distributions were performed by solving the Maxwell equations using the COMSOL Multiphysics (COMSOL Inc., Burlington, MA).

3. Results and Discussion

Figure 1 shows the transmission electron microscope (TEM) images of as-prepared PS-capped Ag and Au nanoparticles. Average diameters of these uniform Ag nanoparticles are 11.9 ± 0.3 nm (**Figure 1a**) and 18.1 ± 0.5 nm (**Figure 1b**) crafted by capitalizing on two star-like PAA-*b*-PS diblock copolymers with different molecular weights of inner PAA blocks, respectively. Similarly, Au nanoparticles with average diameters of 3.2 ± 0.1, 5.1 ± 0.2, 12.2 ± 0.5, and 18.3 ± 0.4 nm (**Figures 1d-1g**) were also obtained by varying the molecular weight of inner PAA blocks of star-like PAA-*b*-PS diblock copolymers. It is noteworthy that the standard deviations of these nanoparticles are all within 5% of their average diameter, signifying that they are monodisperse. The plasmonic absorption of these uniform nanoparticles in toluene was scrutinized by UV-vis absorption spectroscopy measurements, as shown in **Figures 1c** and **1h**, respectively. Several clear trends can be found by comparing the absorption spectra: (i) The plasmonic absorption peak shifted to the shorter wavelength with a decrease of metal nanoparticle diameter. Specifically, the absorption maxima of Ag nanoparticles shifts from 429 nm to 423 nm as the diameter decreases from 18.1 nm to 11.9 nm. Similarly, the peak positions of Au nanoparticles decrease linearly from 527 to 516 nm with the decrease of diameter from 18.3 to 3.2 nm. (ii) As the diameter of metallic nanoparticles decreases, the full-width-at-half-maxima (FWHM) of plasmonic absorption spectra increases. Taking Au nanoparticles as an example, FWHM increases from 51 nm to 62 nm as the diameter decreases from 18.3 nm to 3.2 nm. (iii) Compared with Au nanoparticles, Ag nanoparticles possesses the more obvious plasmonic absorption peak in visible region due to a distinct valley at approximately 315 nm separating the visible absorption from the ultraviolet absorption. Furthermore, we studied the effect of ligands (i.e., PS chains and small molecules oleylamine) attached to the nanoparticle surface on the plasmonic absorption of metallic nanoparticles. **Figure 2** compares the UV-vis spectra of 18-nm PS-capped Au nanoparticles and oleylamine-capped Au nanoparticles. In comparison with oleylamine-capped Au nanoparticles, the UV-vis spectral peak of PS-capped Au nanoparticles shifts to the longer wavelength.

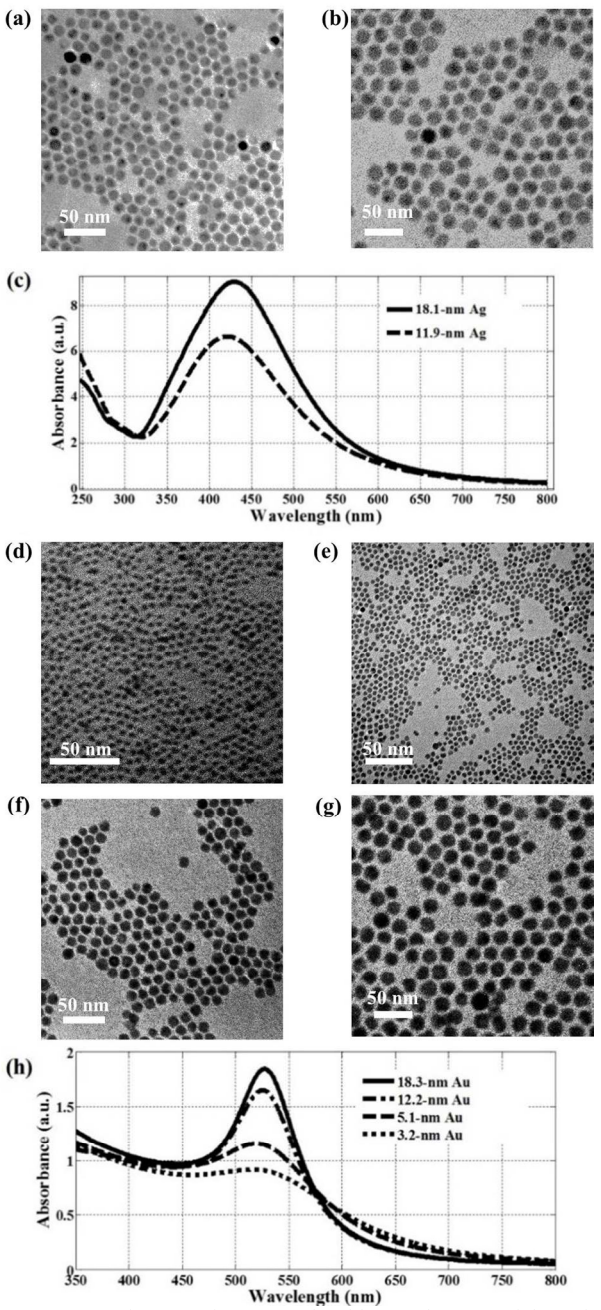

Figure 1. TEM images of PS-capped noble metal nanoparticles using amphiphilic star-like PAA-*b*-PS diblock copolymers as nanoreactors. The diameters of Ag nanoparticles are (a) 11.9 ± 0.3 nm and (b) 18.1 ± 0.5 nm, whereas the diameters of Au nanoparticles are (d) 3.2 ± 0.1 nm, (e) 5.1 ± 0.2 nm, (f) 12.2±0.5 nm, and (g) 18.3±0.4 nm. (c) and (h) UV-Vis spectra for PS-capped Ag and Au nanoparticles, respectively.

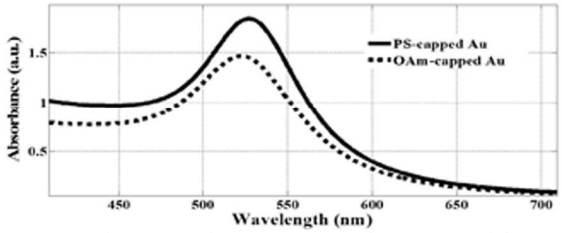

Figure 2. UV-vis spectra of 18-nm PS-capped Au nanoparticles and 18-nm oleylamine-capped Au nanoparticles.

In order to gain insights into the above trends of the plasmonic absorptions and effects of the intra- and inter-band transitions on the SPR of plasmonic nanoparticles, we calculated the absorption cross-sections of plasmonic nanoparticles via 3-dimensional calculation of electromagnetic field distribution. On the basis of morphologys of as-synthesized nanoparticles, a detailed geometric model was created to represent PS-capped noble metal nanoparticles in toluene, as shown in **Figure 3a**. We note that the refractive indices of toluene and PS-layer were from the literature.[46] The computational domain was artificially truncated by the perfectly matched layer (PLM) originally formulated by Berenger,[47] which can strongly absorb the outgoing waves from the interior of a computational region without reflecting them back into the interior. In addition, the PML was placed sufficiently far from nanoparticle in order to minimize the effect of this artificial boundary. **Figure 3b** provides an example of 3-dimensional mesh dicretization of the model and the electric field around the nanoparticle. Meshing was performed with tetrahedral elements. Considering the characteristic of local electromagnetic field distribution of noble metal nanoparticles, a gradual meshing method was used in the calculation, that is, the mesh around the nanoparticle was extremely finer than the mesh far away from the nanoparticle.

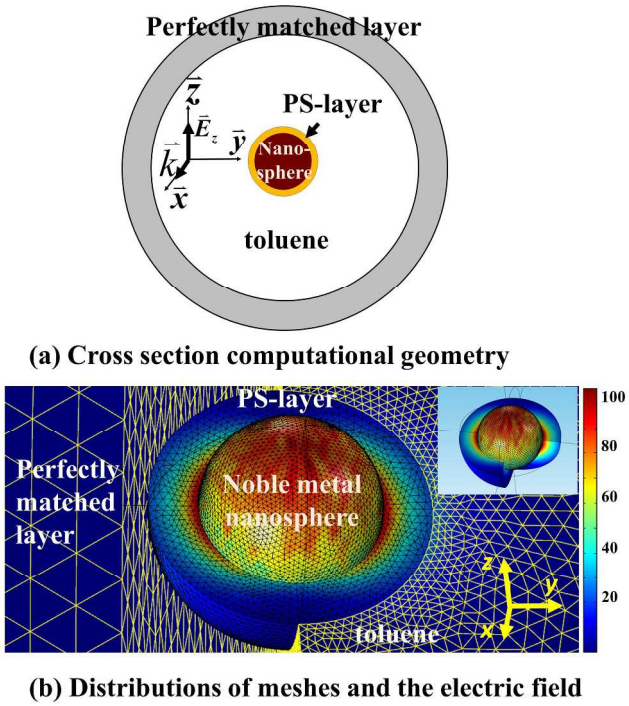

Figure 3. (a) A cross-section of the computational geometry. The calculation dimension is truncated by a perfectly matched layer, which is placed sufficiently far from nanoparticle. The incident wave is polarized along z axis, traveling along x axis. $\overrightarrow{E_z}$ and $\vec{k}$ are the incident electric field and the wave vector, respectively. The medium inside is toluene. The metallic nanoparticle is cladded by a 4-nm PS-layer. (b) Plots of the relative electric field, $\boldsymbol{E} = (\boldsymbol{E}\cdot\boldsymbol{E}^*)^{1/2}/|\boldsymbol{E}_{inc}|$, where $(\boldsymbol{E}\cdot\boldsymbol{E}^*)^{1/2}$ is the amplitude of the total electric field and $|\boldsymbol{E}_{inc}| = 1\,J/nm^2$ is the amplitude of the incident field. The Au nanoparticle shown is 18-nm in diameter cladded by a 4-nm PS-layer. The view angle is shown by a 3D coordinate on the bottom right. The insert on the top right shows the electric field surrouding the nanoparticle on both xy and yz planes.

The plasmonic absorption of visible light of Ag and Au nanoparticles has been recognized due to the intra-band transitions of free-electrons,[48] to which our theoretical calculations has afforded the convincing evidences. $\varepsilon_2(\omega)$ was first set as the imaginary component of $\varepsilon_{intraband}(\omega)$ without considering the contribution of the inter-band transitions. The electromagnetic field calculations were carried out using the finite element method. **Figure 4a** and **4b** show the absorption cross-sections of PS-capped Ag and Au nanoparticles, respectively. The peak intensities were normalized for comparison. Obviously, the peak positions and the trends of peak blue-shifting and broadening with the decreased nanoparticle sizes are consistent with that of the measured spectra in **Figure1**. Moreover, the influence of the cladding (capping) of Au nanoparticles on the plasmonic absorption peak was investigated by the numerical calculation based on $\varepsilon_{intraband}(\omega)$. The oleylamine-capped Au nanoparticles were regarded as bare Au nanoparticles in simulation owing to the negligible influence of oleylamine on the optical field.[49,50] **Figure 4c** shows a comparison between the simulated absorption cross-section of PS-capped Au nanoparticles and that of bare Au nanoparticles. The simulated absorption peak of PS-capped Au nanoparticles shifts to the longer wavelength, which is consistent with the measured spectra (**Figure 2**). On the other hand, with regard to the inter-band transition, the reported resonance frequencies of Ag films expressed by wavelength using $1240/frequency(eV)$ are of 1519.4, 276.7, 151.5, 136.5, 061.1 nm and that of Au films are 2987.6, 1493.8, 417.6, 288.1, 93.1 nm.[38] These wavelengths are far away from the measured plasmonic absorption peaks in the visible region (i.e., 429 nm for 18-nm Ag and 527 nm for 18-nm Au as shown in **Figure 1**). This indicates that the inter-band transition is not a major contributor to the plasmonic absorption in the visible region. Taken together, the results described above show that the plasmonic absorption of Ag and Au nanoparticles in the visible region originates from the intra-band transition of free-electrons.

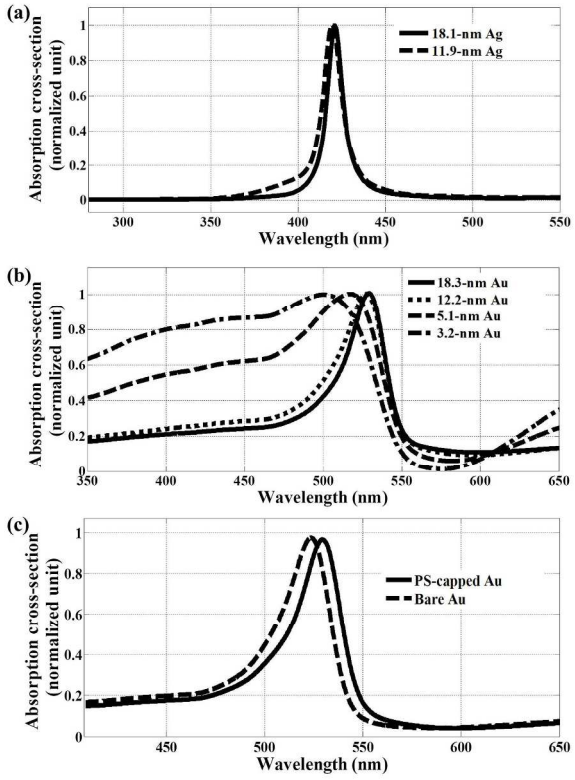

Figure 4. The simulated absorption cross-sections of (a) PS-capped Ag nanoparticles with diameters of 11.9 and 18.1 nm, (b) PS-capped Au nanoparticles with diameters of 3.2, 5.1, 12.2, and 18.3 nm, and (c) 18-nm Au nanoparticles capped with PS or oleylamine (i.e., bare Au). The value of $\varepsilon_2(\omega)$ equaled the imaginary component of $\varepsilon_{intraband}(\omega)$.

This journal is © The Royal Society of Chemistry 2013

It is worth noting that the amplitude of the calculated absorption cross-sections in **Figure 4** descended in the ultraviolet region, signifying that the absorption band in the ultraviolet region in the measured spectra is not due to intra-band transitions. We then set $\varepsilon_2(\omega)$ as the imaginary of $\varepsilon_{intraband}(\omega) + \varepsilon_{interband}(\omega)$ and calculated the absorption cross-sections of PS-capped Ag and Au nanoparticles again. The calculations are shown in **Figure 5**. Intriguingly, exactly as in the measured spectra, the absorption intensity in the ultraviolet region enhances in the calculated absorption cross-sections. Therefore, the inter-band transition is a major contributor to the spectral absorption in the ultraviolet region. Meanwhile, it is noticeable that when the reported resonance frequencies ω_j (in equation (1)) derived from Ag and Au films[38] were utilized as that of Ag and Au nanoparticles, respectively, the simulated absorption intensities of both in the ultraviolet region were much higher than the measured ones, illustrated by the dotted curves in **Figure 5a** and **5b**, respectively. The inter-band transition with frequency closest to the visible frequency has a great influence on the plasmonic absorption peak in the visible region. For Ag, the reported inter-band transition closest to the plasmonic absorption peak of the visible region is at around 276.7 nm (i.e., 4.481 eV denoted by ω_{1Ag}), approximately 153 nm away from the plasmonic absorption peak at 427 nm. For Au, on the other hand, the closest inter-band transition to visible region was reported at 417.6 nm (i.e., 2.969 eV denoted by ω_{1Au}), approximately 109 nm away from the plasmonic absorption peak at 527 nm. Clearly, compared with Au, the inter-band transition of Ag has less influence on the plasmonic absorption in the visible region. This also explains why the plasmonic absorption at optical frequencies of Ag nanoparticles is more obvious than that of Au nanoparticles. It is well-known that compared with film or bulk materials, the band gap of nanoparticle increases. Thus, the resonance frequency of inter-band transition should shift to the higher frequency. In light of our experimental measurements, for both Ag and Au, we attempted to obtain the resonance frequencies of inter-band transition closest to the plasmonic absorption peaks in the visible region. The resonance frequencies of the inter-band transition in Ag or Au nearest to the plasmonic absorption peak of visible light are represented by the sum of the reported resonance frequency of Ag or Au film and the increment (Δ), i.e., $\omega_{1Ag} + \Delta$ for Ag, and $\omega_{1Au} + \Delta$ for Au. The absorption cross-sections of Ag and Au nanoparticles with 18-nm diameter were calculated using different Δ and were compared with the measured ones, as shown in **Figure 5a** and **5b**, respectively. As Δ increases, the calculated absorption intensity at the ultraviolet region decreases and the valley near ultraviolet region shifts to the shorter wavelength, which is much consistent with the measured one. This indicates that the frequency of inter-band transitions of Ag and Au nanoparticles is larger than that of Ag and Au films. Therefore, in Ag or Au nanoparticles, the influence of inter-band transitions in ultraviolet region on the plasmonic absorption of visible light is weaker than it is in Ag or Au films.

Based on the above analysis, in $\varepsilon_{interband}(\omega)$ the inter-band transition frequencies closest to the visible region are suggested to be 4.981 eV for Ag nanoparticles and 3.669 eV for Au nanoparticles, which are higher than the reported values (4.481 eV for Ag film and 2.969 eV for Au film). According to the optimized dielectric function $\varepsilon(\omega)$, the absorption cross-sections of PS-capped Ag and Au nanoparticles with various sizes were calculated again, as shown in **Figure 5c** and **5d**, respectively. Clearly, from the ultraviolet to visible region, not only the peak position and the trend of peak shifting or broadening with nanoparticle sizes but also the shape of absorption curves are consistent with those of the measured spectra.

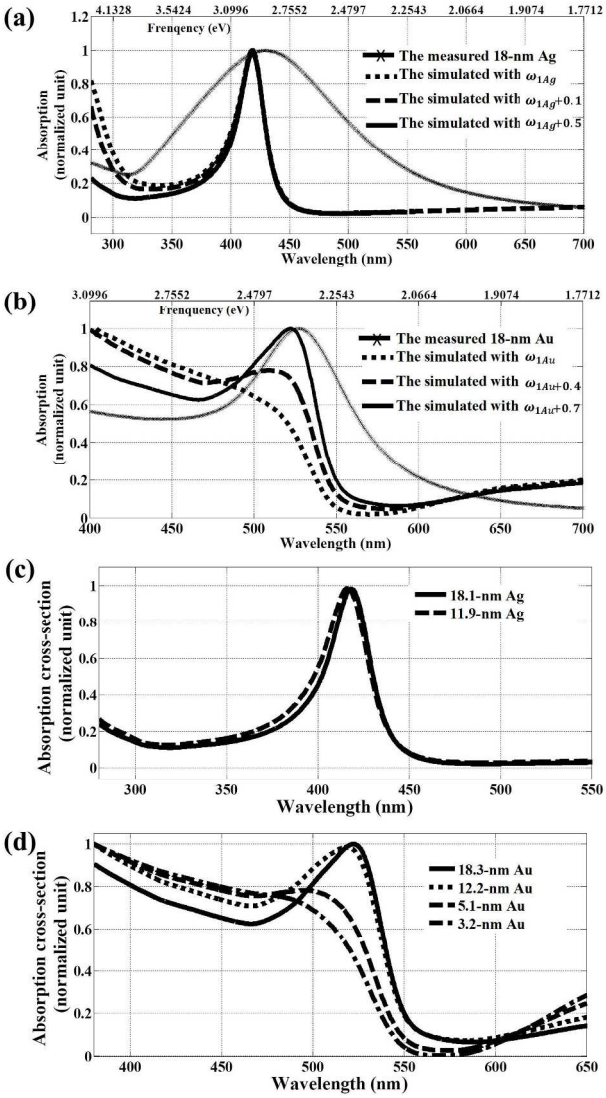

Figure 5. Simulated absorption cross-sections according to $\varepsilon(\omega) = \varepsilon_{intraband}(\omega) + \varepsilon_{interband}(\omega)$: (a) 18-nm PS-capped Ag nanoparticles with the resonance frequencies of ω_{1Ag}, $\omega_{1Ag} + 0.1\,eV$, and $\omega_{1Ag} + 0.5\,eV$; (b) 18-nm PS-capped Au nanoparticles with the resonance frequencies of ω_{1Au}, $\omega_{1Au} + 0.4\,eV$, and $\omega_{1Au} + 0.7\,eV$. ω_{1Ag} and ω_{1Au} are the resonance frequencies of Ag and Au films, respectively, reported in the literature.[38] A representative experimental spectrum is also presented in both (a) and (b) for comparison. Simulated absorption cross-sections based on the optimized inter-band transition frequencies in $\varepsilon(\omega)$: (c) PS-capped Ag nanoparticles with diameters of 11.9 and 18.1 nm; (d) PS-capped Au nanoparticles with diameters of 3.2, 5.1, 12.2, and 18.3 nm.

On the basis of the measured and simulated results described above, we scrutinized the size- and environment-dependence of peak position and width of plasmonic absorption spectra**.** For small enough particles, the discrete characteristics of the electronic energy levels within energy band become obvious. The average electronic energy level spacing of successive quantum levels δE, known as Kubo gap, is given by $\delta E = 4E_f/3m$, where E_f is the Fermi energy of the bulk material and m is total number of electrons in a nanocrystal.[51] Clearly, the smaller nanoparticle has a smaller m, and thus a larger δE. Therefore, the absorption energies of free-electron transitions within the energy band (the

sp-band for Ag and Au) are blue-shifted with decreasing nanoparticle size. Additionally, the fact that the plasmonic absorption spectrum broadens with the decreased nanoparticle sizes can be rationalized by the Mie theory.[43] The full width at half maximum (FWHM, Γ) is given by the phenomenological damping constant $\gamma = \gamma_{D0} + \frac{AV_f}{L_{eff}}$ by combining Mie theory and equation (2), i.e., $\Gamma \approx \gamma.52$ Obviously, the damping constant increases with a decrease of nanoparticle size due to the stronger surface scattering of free-electrons, and so does the FWHM.

Moreover, we investigated the red-shift of plasmonic absorption peak caused by the PS-claddings of nanoparticles. It is clear that the shift trend of the simulated absorption spectra agree with the experimental observations, as shown in **Figure 2** and **Figure 4c**, respectively. As all parameters related to the Au nanoparticle including the dielectric constant, dimension, and morphology remained unchanged in simulation, the red-shift should be due to the cladding (i.e., capping) material on the Au nanoparticle surface rather than the Au nanoparticle itself. The influence of the cladding material on the plasmonic absorption peak can be elucidated as follows. As all the material parameters of an Au nanoparticle are fixed, the wavelength of light which excites the plasmonic resonance absorption of Au nanoparticle (denoted λ_p) can be determined. A dielectric wavelength of light is $\frac{\lambda_0}{n}$, where λ_0 and n are the vacuum wavelength and refractive index of the dielectric, respectively. In the toluene solution, the λ_p light wave induces the plasmonic resonance absorption of the Au nanoparticle, resulting in $\frac{\lambda_0}{n_{toluene}} = \lambda_P$, i.e., the vaccum wavelength of exciting plasmonic resonance absorption of the Au nanoparticle is $\lambda_0 = n_{toluene} \cdot \lambda_P$. Similarly, in the cladding of PS dielectric, the vaccum wavelength to excite plasmonic resonance absorption of the Au nanoparticle is $\lambda_0 = n_{PS} \cdot \lambda_P$. The refractive index of PS (n_{PS}=1.59) is larger than that of toluene ($n_{toluene}$ =1.49). Consequently, as the vacuum wavelength is an independent variable, a red-shift of the absorption peak of the PS-capped Au nanoparticle was thus observed. Such a characteristic of the plasmonic absorption of noble metal may be applied for accurate measurement of the refractive index of medium.

4. Conclusion

In summary, monodisperse Ag and Au nanoparticles with different diameters were synthesized using amphiphilic star-like diblock copolymers as nanoreactors. On the basis of the experimentally measured plasmonic absorption spectra of synthesized Ag and Au nanoparticles, 3-dimensional finite element calculation was performed. The calculated absorption spectra well reproduced the experimental observations. Combining the experiments and 3-dimensional finite element calculations, the contribution of intra-band transitions and inter-band transitions to the plasmonic absorption of Ag and Au nanoparticles was scrutinized. The intra- and inter-band transitions were found to contribute primarily to the visible and ultraviolet absorption spectra, respectively. Meanwhile, the influences of nanoparticle sizes and surface ligands on the plasmonic absorption were systematically investigated. As the diameter of metallic nanoparticles decreased, the plasmonic absorption peak shifted to the shorter wavelength, whereas the FWHM increased. In addition, PS chains tethered on the metal nanoparticle surface caused a red-shift of the plasmomic absorption peak. Such experimentally observed size- and environment-dependence of the peak position and width of plasmonic absorption spectra were also investigated theoretically.

Acknowledgements

We gratefully acknowledge funding support from the National Science Foundation (CMMI 1562075 and 1727313; DMR 1709420), the Air Force Office of Scientific Research (FA9550-16-1-0187), the National Science Foundation of China (61875234, 61775245 and 61627814), and the National Study Fund Committee (Project number: 2016-QT-049).

†Electronic supplementary information (ESI) available: See DOI: 10.1039/c1ee00000x.

References

(1) Bastus, N. G.; Piella, J.; Puntes, V. *Langmuir* **2016**, *32*, 290.
(2) Dastmalchi, B.; Tassin, P.; Koschny, T.; Soukoulis, C. M. *Advanced Optical Materials* **2016**, *4*, 177.
(3) Zaleska-Medynska, A.; Marchelek, M.; Diak, M.; Grabowska, E. *Advances in Colloid and Interface Science* **2016**, *229*, 80.
(4) Zaleski, S.; Wilson, A. J.; Mattei, M.; Chen, X.; Goubert, G.; Cardinal, M. F.; Willets, K. A.; Van Duyne, R. P. *Accounts of Chemical Research* **2016**, *49*, 2023.
(5) Haran, G. *Accounts of Chemical Research* **2010**, *43*, 1135.
(6) Wang, W.; Wang, S.; Liu, Q.; Wu, J.; Tao, N. *Langmuir* **2012**, *28*, 13373.
(7) Zhang, Y.; Gu, C.; Schwartzberg, A. M.; Chen, S.; Zhang, J. Z. *Physical Review B* **2006**, *73*, 165405.
(8) Ong, W. L.; Gao, M.; Ho, G. W. *Nanoscale* **2013**, *5*, 11283.
(9) Ozbay, E. *Science* **2006**, *311*, 189.
(10) Tan, C. F.; Ong, W. L.; Ho, G. W. *ACS Nano* **2015**, *9*, 7661.
(11) Gao, M.; Connor, P. K. N.; Ho, G. W. *Energy & Environmental Science* **2016**, *9*, 3151.
(12) Xu, H.; Käll, M. *Physical Review Letters* **2002**, *89*, 246802.
(13) Baghbanzadeh, M.; Carbone, L.; Cozzoli, P. D.; Kappe, C. O. *Angewandte Chemie International Edition* **2011**, *50*, 11312.
(14) Sheldon, M. T.; van de Groep, J.; Brown, A. M.; Polman, A.; Atwater, H. A. *Science* **2014**.
(15) Chen, Y.; Yang, D.; Yoon, Y. J.; Pang, X.; Wang, Z.; Jung, J.; He, Y.; Harn, Y. W.; He, M.; Zhang, S.; Zhang, G.; Lin, Z. *Journal of the American Chemical Society* **2017**, *139*, 12956.
(16) Xiao, J.; Qi, L. *Nanoscale* **2011**, *3*, 1383.
(17) Linic, S.; Christopher, P.; Xin, H.; Marimuthu, A. *Accounts of Chemical Research* **2013**, *46*, 1890.
(18) Park, J.; Joo, J.; Kwon, S. G.; Jang, Y.; Hyeon, T. *Angewandte Chemie International Edition* **2007**, *46*, 4630.
(19) Leong, W. L.; Lee, P. S.; Lohani, A.; Lam, Y. M.; Chen, T.; Zhang, S.; Dodabalapur, A.; G. Mhaisalkar, S. *Advanced Materials* **2008**, *20*, 2325.
(20) Darling, S. B. *Progress in Polymer Science* **2007**, *32*, 1152.
(21) Rodríguez-Hernández, J.; Chécot, F.; Gnanou, Y.; Lecommandoux, S. *Progress in Polymer Science* **2005**, *30*, 691.
(22) Pang, X.; Zhao, L.; Han, W.; Xin, X.; Lin, Z. *Nat Nano* **2013**, *8*, 426.
(23) Chen, Y.; Yoon, Y. J.; Pang, X.; He, Y.; Jung, J.; Feng, C.; Zhang, G.; Lin, Z. *Small* **2016**, *12*, 6714.
(24) Christ, A.; Zentgraf, T.; Kuhl, J.; Tikhodeev, S. G.; Gippius, N. A.; Giessen, H. *Physical Review B* **2004**, *70*, 125113.
(25) Grześkiewicz, B.; Ptaszyński, K.; Kotkowiak, M. *Plasmonics* **2014**, *9*, 607.
(26) Maegawa, S.; Matsuoka, H.; Fukui, S.; Itoigawa, F.; Nakamura, T. *Tribology Letters* **2016**, *64*, 7.
(27) Hartland, G. V. *Chemical Reviews* **2011**, *111*, 3858.

 This journal is © The Royal Society of Chemistry 2013

(28) Yadgarov, L.; Choi, C. L.; Sedova, A.; Cohen, A.; Rosentsveig, R.; Bar-Elli, O.; Oron, D.; Dai, H.; Tenne, R. *ACS Nano* **2014**, *8*, 3575.
(29) Davletshin, Y. R.; Lombardi, A.; Cardinal, M. F.; Juvé, V.; Crut, A.; Maioli, P.; Liz-Marzán, L. M.; Vallée, F.; Fatti, N. D.; Kumaradas, J. C. *ACS Nano* **2012**, *6*, 8183.
(30) Yang, D.; Pang, X.; He, Y.; Wang, Y.; Chen, G.; Wang, W.; Lin, Z. *Angewandte Chemie International Edition* **2015**, *54*, 12091.
(31) Ray, P. C. *Chemical Reviews* **2010**, *110*, 5332.
(32) Mazzucco, S.; Geuquet, N.; Ye, J.; Stéphan, O.; Roy, W. V.; Dorpe, P. V.; Henrard, L.; Kociak, M. *Nano Letters* **2012**, *12*, 1288.
(33) Siabi-Garjan, A.; Savaloni, H. *Plasmonics* **2015**, *10*, 1.
(34) Fernándezhernández, R. C.; Gleasonvillagran, R.; Torrestorres, C.; Rodríguezfernández, L.; Crespososa, A.; Cheangwong, J. C.; Lópezsuárez, A.; Rangelrojo, R.; Oliver, A.; Reyesesqueda, J. A. *Journal of Optics* **2012**, *14*, 125203.
(35) Han, S.; Kim, H.; Kim, Y. W.; Kim, Y.-J.; Kim, S.; Park, I.-Y.; Kim, S.-W. *Nature Communications* **2016**, *7*, 13105.
(36) Govorov, A. O.; Zhang, H.; Demir, H. V.; Gun'Ko, Y. K. *Nano Today* **2014**, *9*, 85.
(37) Chen, Y.; Wang, Z.; He, Y.; Yoon, Y. J.; Jung, J.; Zhang, G.; Lin, Z. *Proceedings of the National Academy of Sciences* **2018**, *115*, E1391.
(38) Rakić, A. D.; Djurišić, A. B.; Elazar, J. M.; Majewski, M. L. *Appl. Opt.* **1998**, *37*, 5271.
(39) Drude, P. *Annalen Der Physik* **2006**, *308*, 369.
(40) Kreibig, U.; Vollmer, M. *Optical Properties of metal clusters*; 1995 ed.; Springer-Verlag Berlin Heidelberg: Germany, 1995.
(41) Zeman, E. J.; Schatz, G. C. *The Journal of Physical Chemistry C* **1987**, *91*, 634.
(42) Baida, H.; Billaud, P.; Marhaba, S.; Christofilos, D.; Cottancin, E.; Crut, A.; Lermé, J.; Maioli, P.; Pellarin, M.; Broyer, M.; Del Fatti, N.; Vallée, F.; Sánchez-Iglesias, A.; Pastoriza-Santos, I.; Liz-Marzán, L. M. *Nano Letters* **2009**, *9*, 3463.
(43) Hu, M.; Novo, C.; Funston, A.; Wang, H.; Staleva, H.; Zou, S.; Mulvaney, P.; Xia, Y.; Hartland, G. V. *Journal of materials chemistry* **2008**, *18*, 1949.
(44) Kreibig, D. P. U. *Zeitschrift für Physik A Hadrons and Nuclei* **1970**, *234*, 307.
(45) Muskens, O. L.; Bachelier, G.; Fatti, N. D.; Vallée, F.; Brioude, A.; Jiang, X.; Pileni, M.-P. *The Journal of Physical Chemistry C* **2008**, *112*, 8917.
(46) Samoc, A. *Journal of Applied Physics* **2003**, *94*, 6167.
(47) Berenger, J.-P. *Journal of Computational Physics* **1994**, *114*, 185.
(48) Noguez, C. *Journal of Physical Chemistry C* **2007**, *111*, 3806.
(49) Vodnik, V. V.; Božanić, D. K.; Džunuzović, E.; Vuković, J.; Nedeljković, J. M. *European Polymer Journal* **2010**, *46*, 137.
(50) Ochiai, M.; Nishi, Y.; Goto, S.; Frohn, H. J. *Angewandte Chemie International Edition* **2005**, *44*, 406.
(51) Kreibig, U. *Journal of Physics F Metal Physics* **2001**, *4*, 999.

Cite this: DOI: 10.1039/c1ee00000x

www.rsc.org/ees

PAPER

The table of contents entry

An integrated experimental and theoretical study on optical properties of uniform hairy noble metal nanoparticles

Di Yang,[†,1] Yihuang Chen,[†,2] Hongshang Peng,[1] Gengxiang Chen, [1] Zhiqun Lin[*,2]

†Equal contribution

[1]School of Science, Minzu University of China, Beijing 100081, China

[2]School of Materials Science and Engineering, Georgia Institute of Technology, Atlanta, GA 30332

Keywords: amphiphilic star-like copolymers; nanoreactors; plasmonic nanoparticles; intra-/inter-band transitions; optical properties

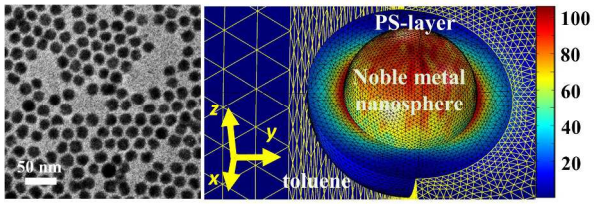

One sentence, of maximum 20 words, highlighting the novelty of the work:

An integrated experimental and modeling study reveals the contributions of intra- and inter-band transitions and the size and surface ligand effects on plasmonic absorption.